J Nanostruct 12(4): 1021-1033, Autumn 2022

RESEARCH PAPER

Adsorption Capacity of Some Metal Ions Using Polyurethane Modified Magnetic Nanoparticles as Adsorbent

*Noor Sabah khadim, Hind M. Saleh *, Nisreen AbdulKareem Abdulaali*

Department of Chemistry, College of Science, University of Misan, Maysan, Iraq

ARTICLE INFO

Article History:
Received 17 July 2022
Accepted 26 September 2022
Published 01 October 2022

Keywords:
Adsorption
Cobalt (II) Ion
Magnetic Nanoparticles
Nickel (II) ion
Polyurethane

ABSTRACT

The current research was designed to study the adsorption of Cobalt Co (II) and Nickel Ni (II) on the surface of modified polyurethane-magnetic nanoparticles (PU-MNPs) as adsorbent. The adsorbent was characterized using a variety of techniques including Fourier Transform Infrared Spectroscopy (FTIR), Atomic Absorption Spectroscopy (AAS), Field Emission Scanning Electron Microscope (FESEM), Dispersive X-Ray Detection (EDX and) Transmission Electron Microscopy (TEM). Different parameters were studied to obtain the best results such as pH, contact time, the concentration of initial metals and temperature. The highest results were obtained at a pH of 5 for Cobalt ions, and at a pH of 7 for Nickel ions. The minimum contact time was 120 min for Cobalt ions and 60 min for Nickel ions. The initial concentration was 150 mg/g for Co ions and 250 mg/g for Ni ions, and 300 agitation rpm speed at temperature 25±2 °C, which was 82% and 94% for Cobalt and Nickel ions respectively. The results showed that the adsorption follows the Lankmayr and Freundlich equations. It was noticed that the Cobalt Co (II) and Nickel Ni (II) ions both followed the Langmuir isotherms. The maximum adsorption of Co (II) was higher than that of Ni (II).

How to cite this article
Khadim N S., Saleh H M., Abdulaali N A. Adsorption Capacity of Some Metal Ions Using Polyurethane Modified Magnetic Nanoparticles as Adsorbent. J Nanostruct, 2022; 12(4):1021-1033. DOI: 10.22052/JNS.2022.04.023

INTRODUCTION

Polyurethane (PU) is one of the most frequently used and known polymers in the world, with annual output estimated to be around 28 million tons in 2020 [1]. The total spread in Europe was on the level of roughly 4 million tons in 2017 and 2018, while the recent total spread outside Europe was to the tune of 2 million tons [2]. The condensed polymerization reaction between polyisocyanates and polyols produces polyurethane [3], and polyurethane is produced when OH alcohol and isocyanate react with NCO. In the present study, polyurethane is made by reacting isocyanates with homo-cyclic azo compounds, which have two groups connected by a homogeneous ring at one end, therefore, the bond varies depending on the type of ring or substituent group that connects the azo group's sides [4]. Since there are no other binding sites available, the nitrogen atom of the azo bridge is the sole one available for bonding with transitional or comparable metal ions [5]. Rings can be substituted with one or more acidic or basic groups such as (-NH_2, -NHR) or (-OH, -SH, -COOH, etc.), the others can contain both categories in a single loop [6]. Isocyanate is a polyurethane component that can be divided into two types of aromatic materials: toluene diisocyanate (TDI) and methylene diisocyanate (MDI). Even though

* *Corresponding Author Email: hind1980@uomisan.edu.iq*

thermoplastic polyurethane is employed in several industries, the majority of Polyurethane – is hard thermoplastic. The polymers resist remelting and reformulation due to thermally cross-linked linkages, and therefore, they are widely used in manufacturing processes. Mechanical processing is not used on thermoplastic polymers like polyethylene or polystyrene.

Methods such as re-milling, bonding, glue pressing, pressure molding, and particle injection limit the use of polyurethane. Fused polyurethane polymer monomer resin or extra isocyanate [7-9] Heavy metals are extremely soluble in aquatic environments, allowing them to be easily absorbed by living organisms. According to previous research, heavy metals were found in the gills, liver tissue, and muscle of many fish species in polluted marine habitats [10]. These metals may wind up accumulating in the human body because of the food chain [11]. The permissible safe limits for heavy metals are connected to when implemented in industries because the majority of heavy metal bands are on a large range of possibilities [12]. Human health risks are lower in food samples [13, 14].

Heavy metals are defined as metallic elements that have a relatively high density compared to water, examples of these metals are metals, Cobalt (Co), and Nickel (Ni). Various methods are used to remove heavy metal ions from aqueous solutions including the adsorption, which have two kinds of techniques: physical and chemical. The initial concentration, acid function, temperature, the character of the adsorbing surface, the equilibrium time, and the solvent are factors that influence the kind of adsorption [16-18].

Magnetic nanoparticles have recently been the focus of several studies because they have promising properties that can be used for stimulation, including nanomaterial-based catalysts, biomedical and tissue-specific targeting, magnetically tunable colloidal photonic crystals, microfluidics, magnetic resonance, magnetic field imaging, data storage, environmental processing, Nano fluids, optical filters, fault sensors, magnetic cooling, and positive sensors [19]. The iron oxide nanoparticles, Fe_3O_4, have attracted the most attention due to their superior magnetic strength. Fe^{3+} evenly across the remaining octahedral and tetrahedral sites. These particles have the characteristic of being highly magnetic, so they can be separated from other solutions using an external magnetic field without using any thermal energy or chemical substances, and therefore can be reused again which reduces the total cost [20]. These nanoparticles are chemically stable [21] and their surface can be easily coated with inorganic, organic, and polymeric materials. There are several methods for preparing magnetite particles (Fe_3O_4), including the liquid-gel method Sol-gel method [22], thermal decomposition [23], hydrothermal method [24], and co-sedimentation method [25]. The current study aimed to use the Fe_3O_4-PU nanoparticles as a potential technique to adsorb some heavy metals from the polluted water.

MATERIALS AND METHODS

Chemicals

All chemical reagents used in this work were analytical high-purity and were used without further purification, including 2-Naphthol (%95, OEM), Sodium Hydroxide (%98, Thomas Baker), Hydrogen chloride (%37, Romil-SA), Chloroform (%99, GCC), Sodium Nitrite (**99%,** B.D.H), P-phenylene Di amine (99**%,** Fisher Chemical), Ethanol absolute (%99.9, Romil-SA), Diphenyl Methane Diisocyanate (%99.5, Industry Engineering Co,.Ltd), Preparation ions solution using Deionized Water, Nickel Nitrate (%98, CDH), Cobalt Nitrate (%99, Thomas Baker), Ferric Chloride Anhydrous (%97, Thomas Baker), Ammonium ferrous sulfate hexahydrate (%99, CDH), Ammonium hydroxide (%98, Shijiazhuang Xinlongwei Chemical Co., Ltd), Methanol (Absolute) (%99.9, Xilong Scientific), N, N-Dimethyl Form amide(%99, CDH).

Methods

Synthesis of iron oxide nanoparticles (Fe_4O_3)

Magnetic iron nanoparticles were prepared by co-precipitation of ferrous ions Fe^{+3} and ferrous Fe^{+2} with ammonium hydroxide solution, according to the equation below [26, 27]:

$$Fe^{2+} + 2Fe^{3+} + 8OH \rightarrow Fe_3O_4 + 4H_2O$$

In this method, 10 mmol (1.6220 gm) of anhydrous ferric chloride ($FeCl_3$) and 5 mmol (gm 1.9608) of ammoniac ferrous sulfate [$(NH_4)_2(FeSO_4)_2.6H_2O$] were dissolved in 150 ml of deionized water, in a flask with a capacity of 500 ml with continuous stirring of this solution using a magnetic stirrer (hot plate with a magnetic stirrer) with heating to a temperature of 90° C, where the

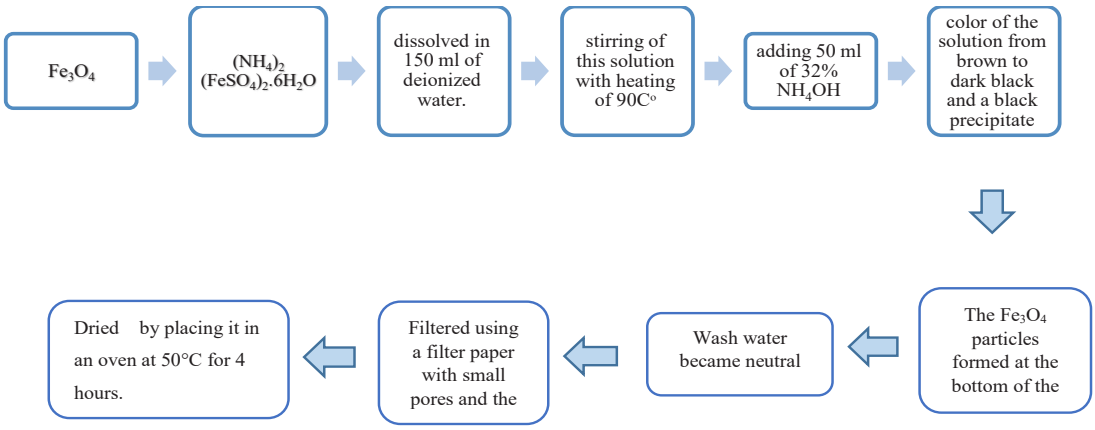

Fig. 1. Flowchart of synthesis technique of magnetic (Fe_3O_4) nanoparticles

chemical precipitation of magnetic nanoparticles of iron (Fe_3O_4) was conducted when adding 50 ml of 32% NH_4OH ammonium hydroxide solution in the form of drops with continuous stirring until the acidity function reaches 10.5-10.0, and when the Fe_3O_4 particles are formed, a change in the color of the solution was noticed from brown to dark black and a black precipitate is formed from magnetic Nano-iron particles (Fe_3O_4NPs**)**. This precipitate was collected using an external magnet. After the solution above it remained transparent, indicating the completion of the sedimentation process as shown in Fig. 1. The increase from the ammonium hydroxide solution, so that the acidity function of the wash water became neutral, then the formed precipitate was filtered using a filter paper with small pores and the resulting precipitate was dried by placing it in an oven at 50°C for 4 hours.

Grafting a polyurethane (PU) polymer on the surface of magnetic iron nanoparticles (Fe_3O_4-PU)

The polyurethane was grafted on the Nano iron oxide (Fe_3O_4) at a certain weight ratio and mixed with the previously prepared azo (1:2), where both are dissolved in chloroform solvent in an amount of (30ml) during mixing, then the mixture is placed in an ultrasonic device (Bath Sonicator) for an hour, so the mixture became homogeneous by the interaction of azo with Nano iron oxide (Fe_3O_4), then MDI is added in an equal amount to the amount of azo mixed with The above nanomaterial and the mixture is placed in the ultrasonic device for half an hour to homogenize the mixture of the polymer components formed with (Fe_3O_4), and to get rid of the solvent, the mixture is placed in a hot plate at a temperature of (50 C°) for (15 minutes) to boil the solvent and volatilize until The precipitate dried brownish-black and to complete the polymerization process, the precipitate is placed in the oven at a temperature of (50 C°) for three hours and then raised to (100 C°) for two hours. The solidification process is completed. It was confirmed by magnets that nanoparticles were mixed with the polymer and the mixture was subtitled to some characterizations such as IR, TEM, FESEM, TEM, and Zeta potential.

Batch adsorption studies

To find the adsorption isotherm by preparing different concentrations of the Adsorbate within the range (of 100-300 mg/L) (50 ml) was added in a series of solutions of heavy metals to (0.025gm) from the prepared (Fe_3O_4-PU) adsorbents, and these solutions were placed in a shaker at a speed of (300) cycles/ minute for 24 hours and upon reaching the equilibrium time and after then separation and clear solutions were measured by atomic absorption spectroscopy and from knowing the values of absorption at the concentration at equilibrium, then finding the amount of the adsorbed substance from the below equation:

$$Qe = (Vsol\ (Co\text{-}Ce))/m$$

Where the initial Concentration is Co، ،(L) Total volume of the adsorbent solution is Vsol, (mg/g) Adsorbent for Final Concentration is Ce، (mg/L) Adsorbent, (mg/g) Adsorbent Quantity is Qe ، (g)

Adsorbent Weight is m.

RESULTS AND DISCUSSION

IR Spectrum of Azo compound, polyurethane PU, Iron oxide nanoparticles Fe_3O_4 and Iron oxide nanoparticles –Polyurethane Fe_3O_4-PU Characterization

The FTIR spectrum of the prepared azo compound showed the effective groups. A strong broadband appears at a frequency of (3452 cm^{-1}) stretching indicating the presence of an (OH group) of the compound (2- naphthole) included in the composition of the resulting compound [28]. The spectrum also showed a weak absorption band at a frequency of (2400 cm^{-1}) belonging to the triple active group (RNC), while the appearance of a peak at frequency (1643) cm^{-1} belongs to the group (N = N) belonging to the azo group [29] as well as two absorption bands at (1539 and 1512 cm^{-1}) overlapping due to the overlapping of two groups (C=N) Fig. 2.

The FTIR spectrum of Polyurethan1 prepared previously paragraph showed the effective aggregates. The spectrum of the compound showed a band at a frequency of (3375 cm^{-1}) stretching belonging to the (N-H) group of polyurethane NHCOO, with the disappearance of the (OH) band at a frequency of (3400 cm^{-1}) belonging to the azo compound involved in the reaction. The frequency (3032 cm^{-1}) belongs to the aromatic C-H group. This indicated that the compound is aromatic. A strong bundle of symmetric stretching appeared at a frequency of (2276 cm^{-1}) indicating the presence of an isocyanate group [30] belonging to polyurethane, as well as the presence of an absorption band at (1708 cm^{-1}) indicating a group (C= O), as well as the appearance of an absorption band and the appearance of a band at (1500 cm^{-1}) indicating a group (C =C) interferes with the beam at a frequency of (1411 cm^{-1}) due to the azo group (N=N) and the appearance of a beam at a frequency of (1200 cm^{-1}) belongs to the group (C-N) and the appearance of a beam at a frequency of (1006 cm^{-1}) on the group (C-O-O) [31] indicates that the compound formed is a polyurethane Fig. 2.

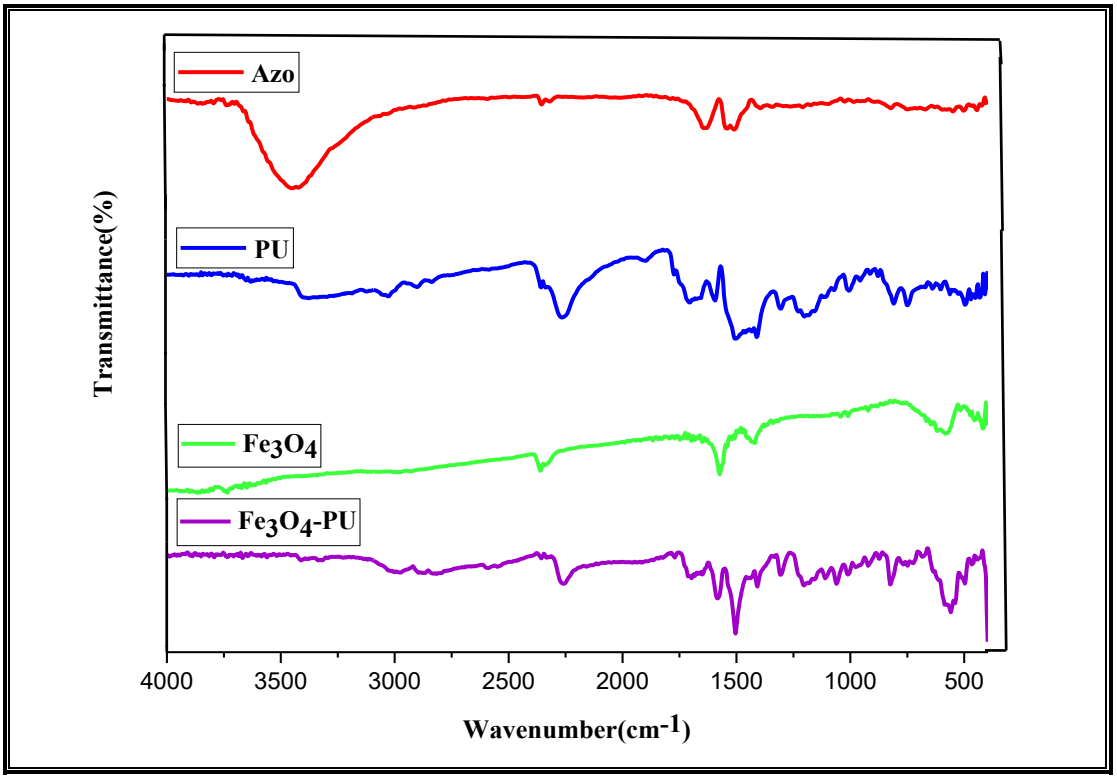

Fig. 2. IR spectrum compounds of: Azo compound, polyurethane PU, Iron oxide nanoparticles Fe_3O_4 and Iron oxide nanoparticles –Polyurethane Fe_3O_4-PU

The FTIR spectrum of the prepared iron oxide nanocomposites (Fe_3O_4 NPs) showed bands at (3402-3618cm^{-1}) due to the amplitude expansion of the O-H bond caused by the ionic water molecules absorbed by the model when washed with it [32]. Also, found a beam at (574,455sh cm-1) that goes back to the (Fe-O) bond, which indicates an expansive expansion for the metal with the oxygen atom in the tetrahedral position and the octahedral position, they represent stretching and bending (and this applies to previous studies [33-34]. The formation of iron oxide nanocrystals is shown in Fig. 2. The FTIR spectrum of the iron oxide nanocomposite (Polyurethane + Fe_3O_4 NPs) revealed a group of (O=C=N) at the site (2260 cm^{-1}) because of the Nano-combination with the polymer. In addition, some bands appeared at (497 and 559 cm^{-1}) due to the (Fe-O) bond at the Tetrahedral and Octahedral sites [35], which indicated that the resulting compound is a Nano polymer (Polyurethane + Fe_3O_4 NPs) as shown in Fig. 2.

XRD Spectrum of Iron oxide nanoparticles and Iron oxide nanoparticles –Polyurethane Characterization

The X-ray diffraction device (Dx-2700B) Haoyuan (Dandong was used, and a Cu-Kα radiation beam with a wavelength (0.15406 nm) and an energy of (30KV) with a current of (20mA, and an angular range of (80-2θ=10). It is shown in Fig. 3a and Fig. 3b. The diffraction pattern in Fig. 3b shows the complete purity and polycrystallization of the Fe_3O_4 NPs and the crystal structure of the nanoparticles is Cubic [36], where the above information corresponds to the standard card (JCPDS File card) No.01-075-1610, It was also noted that the emergence of new peaks different from the spectrum of the nanocomposite and this is due to the bonding of the polymer to the Nano, forming new mixtures with more peaks as noted in the Fig. 3c.

Transmission Electron Microscopy (TEM)

A TEM study was conducted to find out the exact size of the compound, which is the nanostructure property of magnetic nanoparticles MNPs. Such as particle size distribution, size and morphology, the nanoparticles were observed to have typical spherical Fe_3O_4 molecular structure in Nano size Fig. 4a. Magnetic nanoparticles agglomerate due to their high magnetic properties. These results follow the previous studies [37, 38].

Iron oxide NPs in the Nano-polyurethane

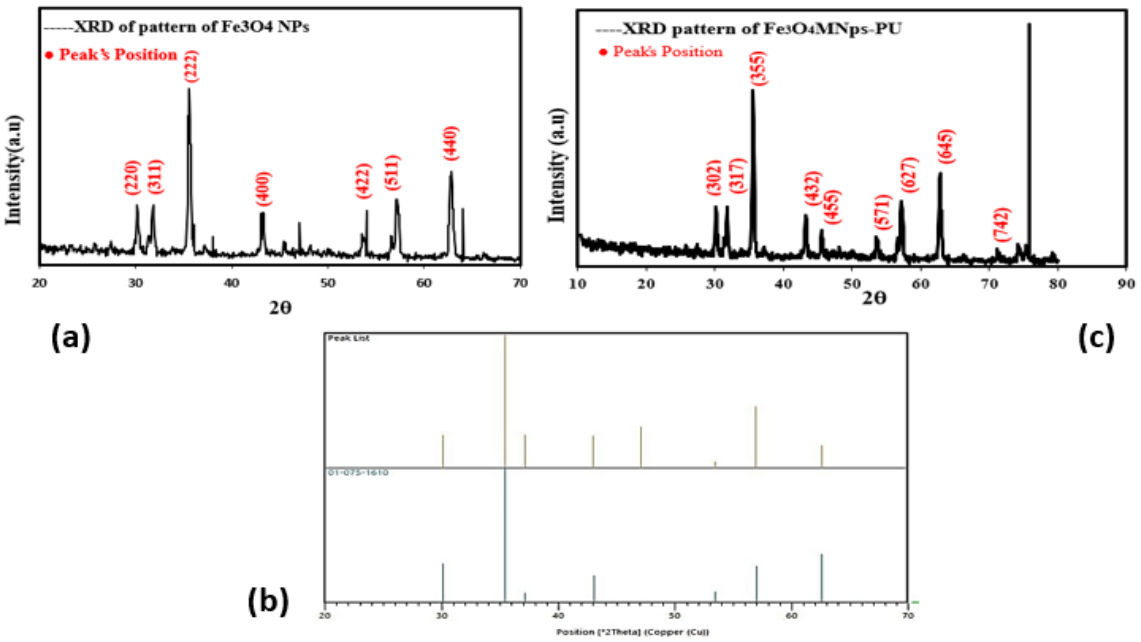

Fig. 3. (a): X-ray Diffraction spectrum of the Fe_3O_4 NPs, (b): Matching the locations of Piatt for the Fe_3O_4 NPs prepared with the locations or angles of the international card numbered (1610-075-01), (c): X-ray Diffraction spectrum of Fe_3O_4 NPs-PU

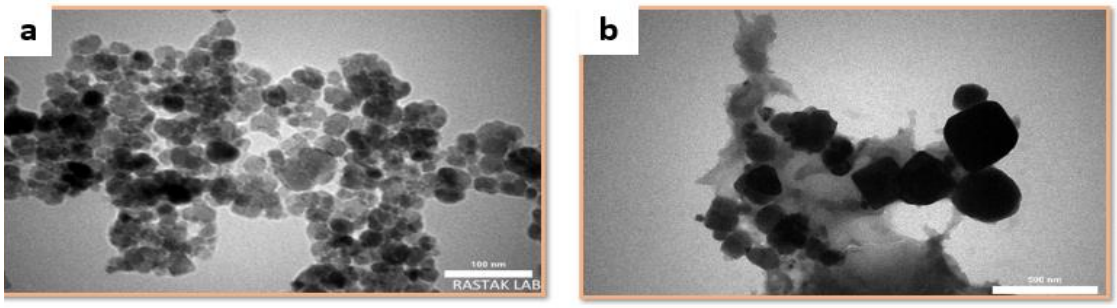

Fig. 4. (a): TEM image of the compound Fe_3O_4 NPs, (b): TEM image of the compound Fe_3O_4-PU

mixture have the characteristic of a large surface-to-volume ratio, and therefore have high surface energies. As a result, they tend to agglomerate to reduce their surface energies [39] Moreover, NPs alone have high chemical activity and are easy to oxidize in the presence of oxygen (especially magnetite) leading to a loss of magnetism or dispersion, but are bound to the polymer it leads to activity Chemically balanced on the surface of the neutral polymer, resulting in increased magnetism and dispersion on the polymer surface. It is necessary to develop an active protection strategy to maintain the stability of these NPs through appropriate surfactant interaction as in the surface of the polymer used in this study [40]. As shown in Fig. 4b.

Field Emission Scanning Electron Microscopy (FESEM)

Scanning electron microscopy (SEM) is one of the most common and widely used methods. Diagnosing nanostructures and nanomaterials, Figs. 5a illustrate microscopic images of the scanning electron microscope (FESEM) of the nanofabricated iron oxide Nano powder. The crystals range in size (from 15-22) nm and the field of view is about (8.6 mm). These results are consistent with XRD measurement and with previous studies [41]. Fig. 5b showed a large-scale gathering of polymer particles around the nanocomposite for Fe_3O_4-PU, and this led to the magnetic dispersal of the nanocomposite due to the presence of the polymer on the outer surface of the iron particles [42], and the resulting surface in both mixtures has a rough and shiny characteristic, the size of the crystal ranges from (15-22) nm and the field of view is about (5.46 mm) in the image.

Fig. 5c shows the spectrum of the energy-dispersive X-ray detector (EDX (attached to FESEM), which is usually used to indicate the composition or chemical analysis of the components of (Nano Iron Oxide), where the spectrum shows distinct peaks at (0.6 keV, 6.5, 7) belong to the iron atom, as well as the appearance of a peak at (0.5 keV) belonging to the oxygen atom, which leads to the formation of iron oxide nanoparticles, and this is consistent with the results of X-ray diffraction (XRD) and previous studies [43].

Zeta potential analysis

Zeta potentials study the surface charge of the particle which affects the agglomeration of nanomaterials and the absorption of ions on the Nano surface [44] Particles with a positive zeta potential of +30 mV or more negative than -30 mV are considered naturally stable. The results showed the presence of one beam for Fe_3O_4 with a value of (mv36.4), with a value of Zeta potential (mv36.4+), and an electrical potential, (cm2/V.S0.000282) as shown in Fig. 6a measured by the scattered light method (ELS), the large positive charge is centered on the surface of the nanocomposite and indicates a high stability and the small iron oxide particles gather on the large charge to form the basic interface of the compound in a stable manner that represents a uniform distribution of nanoparticles as it matches the XRD calculations and previous studies [45].

Figs. 6b show the zeta potential value of (-10.4mv) for (Fe_3O_4-PU). Fe_3O_4 has a positive charge on the surface, which indicates lower affinity stability. To agglomerate over time in groups to form the basic structure, and produce electrostatic forces of attraction to deposit polyurethane on its surface due to the opposite charge of the polyurethane

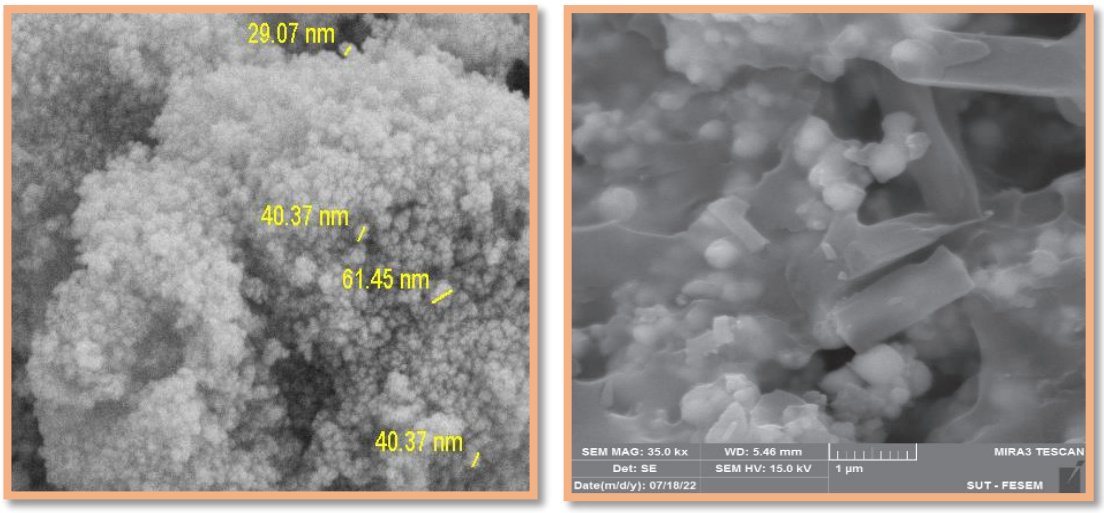

Fig. 5. FESEM images of the compounds: a. Fe_3O_4 NPs, b. Fe_3O_4-PU, and EDX images of the compound of Fe_3O_4 NPs

solution, while the produced Fe_3O_4-PU mixture is characterized by high stability and homogeneity due to the repulsive force between the particles indicated by the huge negative surface charge of the particles by increasing the stability of Fe_3O_4-PU in plankton, the adsorption and removal of various pollutant particles on the surface of polyurethane will be improved [46,47].

Adsorption of heavy metals ions

The adsorption of heavy metal ions, including Cobalt, and Nickel ions, was studied on the surfaces prepared in this study, including nanomonium oxide grafted with polyurethane at the beast ratio (2:1).

Effect of metal ions Concentration

Different Co (II) and Ni (II) ions solutions were prepared; the initial concentrations were as follows 100,150,200,250,300 for Cobalt ion and Nickel ion in order to study the initial concentration effect at room temperature and optimum conditions obtained previously to apply the Langmuir and Freundlich adsorption isotherms. It has been noted that when the initial concentration of the adsorbent material increased, a decrease in the

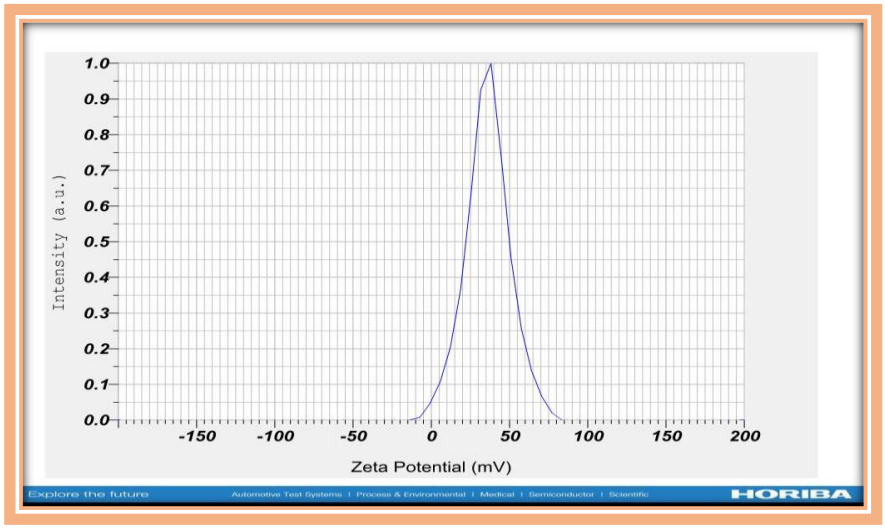

(a)

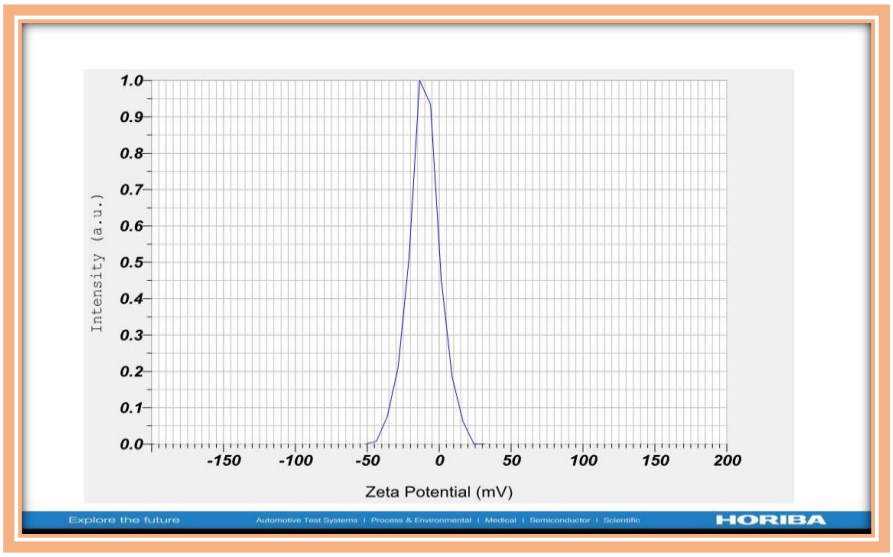

(b)

Fig. 6. (a): ELS Zeta potential for Fe_3O_4 NPs, (b): ELS Zeta potential for Fe_3O_4-PU

removal ratio happened, and an increase in the adsorption capacity may be attributed to the increase in the rate of diffusion and mass transfer on the surface, and then the time required to reach the equilibrium state will be longer. A certain amount of the adsorbent increases with the increase in the initial concentration of the adsorbent at a constant temperature [48].

Equilibrium time

The adsorption process was conducted to calculate the adsorption time of the two mixtures (Fe_3O_4-PU) with heavy metal ions (Co and Ni) and the results showed that the equilibrium time for

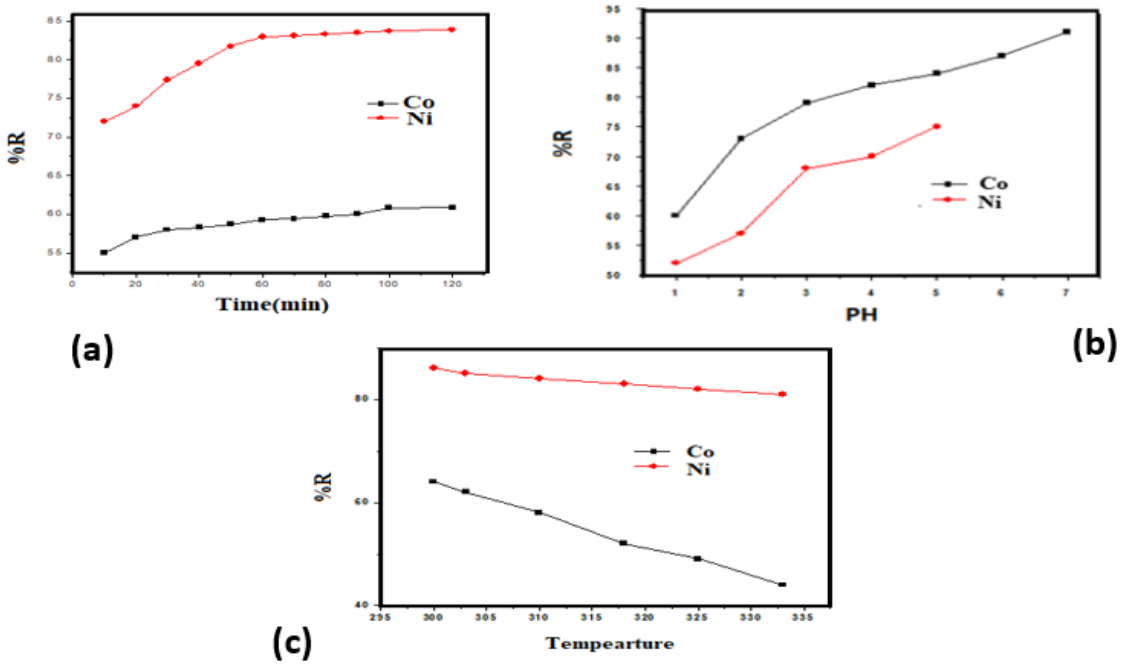

Fig. 7. (a): Equilibrium time curve of Cobalt ion Co (II), Nickel ion Ni (II) element on the surface of the mixture (Fe_3O_4-PU), (b): Effect of acidity function on Cobalt ion Co (II), Nickel ion Ni (II) adsorption on the surface of the mixture (Fe_3O_4-PU), (c): Effect of temperature on Cobalt ion Co (II), Nickel ion Ni (II) adsorption on the surface of the mixture (Fe_3O_4-PU)

Cobalt was (120 min), and the equilibrium time for Nickel (60 min), as shown in Figs. 7a.

While Co^{+2} tends to balance at 120 minutes, and Ni^{+2} tends to the equilibrium state at about 60 minutes then the adsorption becomes constant for each of the ions used in this study, the rapid increase in the percentage removal at the beginning of the adsorption process is due to a large number of vacant adsorbent surfaces on the nanocomposite material Nano iron oxide nanoparticles and polyurethane. This is a faster diffusion of metal ions in the adsorption material [49].

Effect of PH

A study was conducted to study the effect of the acidity function of the adsorption process of heavy metal ions Co and Ni on the prepared surfaces, where we notice that the removal percentage increases with the increase in the amount of the acid function, for example for Cobalt, the maximum adsorption at Co equals 5, While Nickel equals 7, since one end of the polymer has a negative charge, so most of the ions are located in some reaction sites in the adsorbent material due to the presence of competing for positive ions in the solution being acidic and did not exceed the base pH values. This leads to a total reduction of the values of the adsorption sites affinity on the metal ion nanocomposite materials. This is due to the increase in the obstacles to the diffusion of metal ions caused by the positive repulsive forces of the increasing cation at moderate pH values [50] The adsorbent material is relatively negatively charged more than the ionic solution, and this contributes to an increase in Affinity for metal ions at pH values 5 [51], a higher pH (pH > 7) was not used in the current study to avoid removal of metal ions by precipitation as shown in Fig. 7b.

Effect of the Temperature

The degree of adsorption depends on the temperature of the liquid-solid interface. Adsorption studies were performed at different temperatures 300, 303, 310, 318, 325 and 333. The percentage of metal ion removal decreases with increasing temperature. It was found that a lower temperature is possible for the adsorption process. Thus, the process was concluded to be exothermic and automatic. The decrease in the

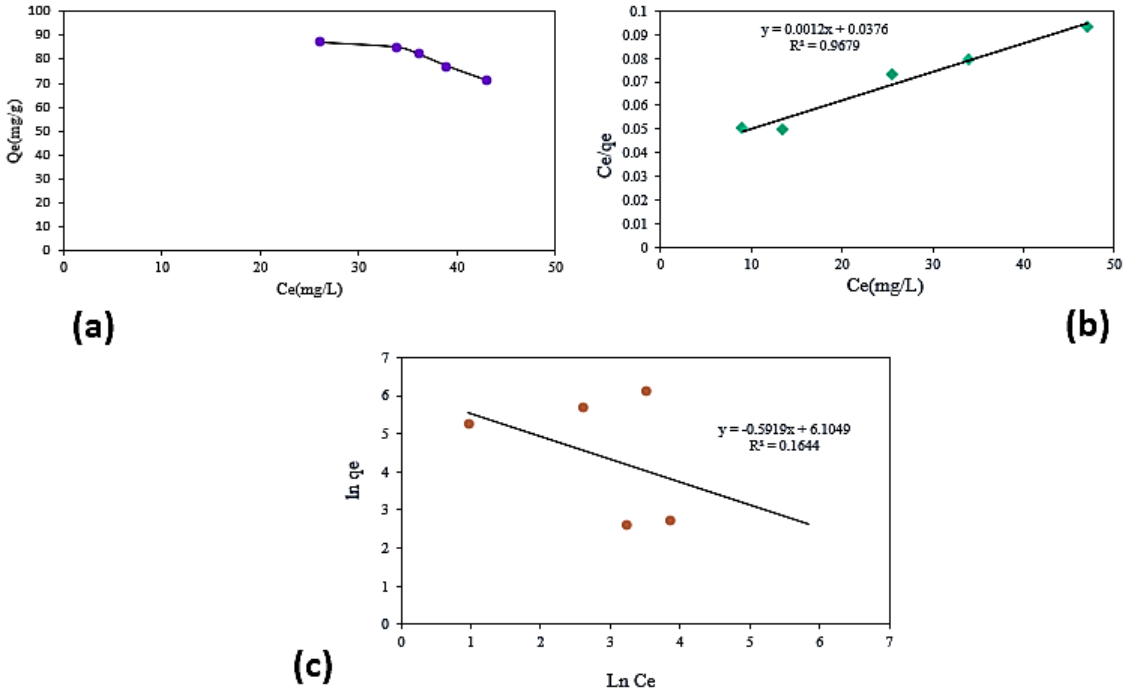

Fig. 8. (a): The percentage of the Cobalt ion Co (II) on the surface of the mixture (Fe_3O_4-PU) at a temperature of C°25, pH 5, and the initial concentration 150mg/ L, (b): Lankemere isotherm for adsorption of the Cobalt ion Co (II) on the surface of the mixture (Fe_3O_4-PU) at a temperature of C°25, pH 5 and the initial concentration 150mg/ L, (c): The Freundlich isotherm for adsorption of the cobalt ion Co (II) on the surface of the mixture (Fe_3O_4-PU) at a temperature of C°25, pH 5 and the initial concentration 150 mg/L

adsorption capacity of nanocomposite materials with increasing temperature is due to the weak bonds carrying metal ions on the adsorbent surfaces of the nanocomposite. The increase in temperature also degrades the regular structure of the nanocomposites materials, which leads to the loss of adsorption sites, thus reducing the removal efficiency of Co (II), and Ni (II) ions. The decrease in the adsorption efficiency with increasing temperature indicates weak bonding interactions between the adsorbent surfaces and the cations; this is an indication that the process can be exothermic and thus leads to the conclusion that the adsorption process was appropriate at lower temperatures as shown in Fig. 7c.

Adsorption Isotherms

Equilibrium uptake of Co^{+2} and Ni^{+2} was investigated with sorption 0.025 gm of (Fe_3O_4-PU) in contact with 50 ml of solution at pH= 5,7 for Co^{+2}, Ni^{+2} and time contact of 120, 60 for Co^{+2}, Ni^{+2} at 25C° temperature. The graphic between Ce versus Ce/ Qe for the compatibility is greater for the Lankemuir model of the Cobalt ion and Nickel ion, which is in agreement with the Lankemuir model (Fig. 7a and 7c), graphic between Ln Ce versus Ln qe (Fig. 7b and 8b) for the Freundlich model. Freundlich equation is used to describe the adsorption characteristics of heterogeneous surfaces, as it considers the presence of effective sites and a heterogeneous adsorption surface and different energies and adsorption in several layers.

RL is indicative of the isotherm shape and predicts whether a sorption system is either favorable (0<R2<1), unfavorable (R2>1) or irreversible (R2=0). Figs. 8a, b and Fig. 9a, 8b give the plots of the Langmuir and Freundlich isotherms of Co^{+2}, Ni^{+2} ions adsorbed onto (Fe_3O_4-PU) respectively, and Table 1. displays qmax, KL, KF, and the correlation coefficient R2 results for the Langmuir and Freundlich isotherms for the adsorption of surface (Fe_3O_4-PU) by the Prepared adsorbents, The results showed that the adsorption follows the Lankemere and Freundlich equations. It was noticed that the Co (II) follow the Lankemuir isotherms, with great value R in the case of Lankemuir isotherm, which indicates that it is chemical adsorption. The Nickel ion Ni (II)

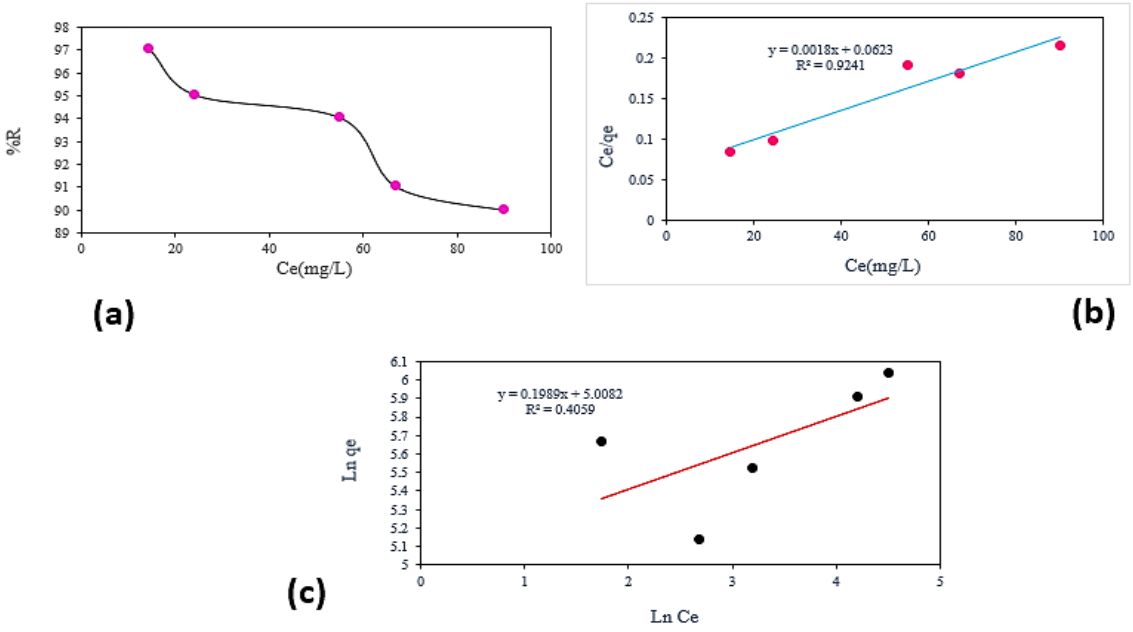

Fig. 9. (a): The percentage of the Nickel ion Ni (II) on the surface of the mixture (Fe_3O_4-PU) at a temperature of C°25, pH 7, and the initial concentration 250mg/ L, (b): Lankemere isotherm for adsorption of the Nickel ion Ni (II) on the surface of the mixture (Fe_3O_4-PU) at a temperature of C°25, pH 7 and the initial concentration 250mg/ L, (c): The Freundlich isotherm for adsorption of the Nickel ion Ni (II) on the surface of the mixture (Fe_3O_4-PU) at a temperature of C°25, pH 7 and the initial concentration 250 mg/ L

Table 1. Lankemuir and Freundlich constants for adsorption of Cobalt, Nickel ions on the surface of the mixture (Fe_3O_4-PU)

Metal ion	Langmuir equation			Freundlich equation		
	K_L	Q max	R^2	K_F	1/n	R^2
Co (II)	0.031915	833.3333	0.9679	0.255918	0.1638	0.1644
Ni (II)	0.035185	526.3158	0.971	1.580884	0.1967	0.4059

also follow the Lankemuir isotherms, with great value R in the case of Langmuir isotherm, which indicates that it is chemical adsorption. Maximum adsorption of Co (II)> Ni (II).

CONCLUSION

The adsorption of heavy metals (Co^{+2}, Ni^{+2}) by (Fe_3O_4-PU) surface has been determined. This study indicates that (Fe_3O_4-PU) have a good capacity for the adsorption of heavy metal ions. The percentage removal depended on pH, Adsorbent concentration and adsorbent dosage. The maximum adsorption capacity was found at pH=5 for Co^{+2}, pH=7 for Ni^{+2}, adsorbent dosage 0.025 gm and initial concentration 150 mg/L for Co^{+2}, initial concentration 150 mg/L for Ni^{+2}, The best contact time within 120, 60min for Co^{+2}, Ni^{+2}. The adsorption process supplied Freundlich and Langmuir, with isotherm models. This material can be successfully used as an environment-friendly

product for the removal of heavy metals from aqueous solutions.

CONFLICT OF INTEREST

The authors declare that there is no conflict of interests regarding the publication of this manuscript.

REFERENCES

1. . Prospectiva Universitaria. 2017;14(1).
2. Pultrusion: A growing market in Europe. Reinforced Plastics. 1991;35(11):44-46.
3. Sharmin E, Zafar F. Polyurethane: An Introduction. Polyurethane: InTech; 2012.
4. Pargai D, Jahan S, Gahlot M. Functional Properties of Natural Dyed Textiles. Chemistry and Technology of Natural and Synthetic Dyes and Pigments: IntechOpen; 2020.
5. Kumar Gupta V. Fundamentals of Natural Dyes and Its Application on Textile Substrates. Chemistry and Technology of Natural and Synthetic Dyes and Pigments: IntechOpen; 2020.
6. Mirjalili BF, Bamoniri A, Rahmati L. One-pot synthesis of 1-amidoalkyl-2-naphthols catalyzed by nano-BF3·SiO2. Arabian Journal of Chemistry. 2019;12(8):2216-2223.
7. Zia KM, Bhatti HN, Ahmad Bhatti I. Methods for polyurethane and polyurethane composites, recycling and recovery: A review. React Funct Polym. 2007;67(8):675-692.
8. Sokolowski SA, Räisänen-Sokolowski AK, Tuominen LJ, Lundell RV. Delayed treatment for decompression illness: factors associated with long treatment delays and treatment outcome. Diving and Hyperbaric Medicine Journal. 2022;52(4):271-276.
9. Nikje MMA, Garmarudi AB, Idris AB. Polyurethane Waste Reduction and Recycling: From Bench to Pilot Scales. Designed Monomers and Polymers. 2011;14(5):395-421.
10. Salim G, Atieqah N, Handayani KR, Indarjo A, Ransangan J. Growth, mortality and exploitation rate of Pampus argenteus, Parastromateus niger and Scomberomorus commerson in Sebatik Waters, Indonesia. Biodiversitas Journal of Biological Diversity. 2020;21(11).
11. Barakat MA. New trends in removing heavy metals from industrial wastewater. Arabian Journal of Chemistry. 2011;4(4):361-377.
12. Mansourri G, Madani M. Examination of the Level of Heavy Metals in Wastewater of Bandar Abbas Wastewater Treatment Plant. Open Journal of Ecology. 2016;06(02):55-61.
13. Sobhanardakani S. Potential health risk assessment of heavy metals via consumption of caviar of Persian sturgeon. Mar Pollut Bull. 2017;123(1-2):34-38.
14. Lahner LL, Franson JC. Lead poisoning in wild birds. Fact Sheet: US Geological Survey; 2009.
15. Wendimu G, Zewge F, Mulugeta E. Aluminium-iron-amended activated bamboo charcoal (AIAABC) for fluoride removal from aqueous solutions. Journal of Water Process Engineering. 2017;16:123-131.
16. Ali SM, Hassun HK, Salih AA, Athab RH, Al-Maiyaly BKH, Hussein BH. Study the properties of Cu_2Se thin films for optoelectronic applications. Chalcogenide Letters. 2022;19(10):663-671.
17. Alia Basma A, Asma A, Oum Elkheir B, Sofiane S. Phreatic aquifer water upwelling: causes, consequences and remedies. Revista Romana de Inginerie Civila/Romanian Journal of Civil Engineering. 2021;12(3):304-313.
18. The Wiki Concept. Wiki: Springer-Verlag. p. 9-30.
19. Hong RY, Li JH, Li HZ, Ding J, Zheng Y, Wei DG. Synthesis of Fe_3O_4 nanoparticles without inert gas protection used as precursors of magnetic fluids. J Magn Magn Mater. 2008;320(9):1605-1614.
20. Bucak S, Yavuzturk B, Demir A. Magnetic Nanoparticles: Synthesis, Surface Modifications and Application in Drug Delivery. Recent Advances in Novel Drug Carrier Systems: InTech; 2012.
21. Zhou W, Tang K, Zeng S, Qi Y. Room temperature synthesis of rod-like $FeC_2O_4{\cdot}2H_2O$ and its transition to maghemite, magnetite and hematite nanorods through controlled thermal decomposition. Nanotechnology. 2008;19(6):065602.
22. Simeonidis K, Mourdikoudis S, Moulla M, Tsiaoussis I, Martinez-Boubeta C, Angelakeris M, et al. Controlled synthesis and phase characterization of Fe-based nanoparticles obtained by thermal decomposition. J Magn Magn Mater. 2007;316(2):e1-e4.
23. Daou TJ, Pourroy G, Bégin-Colin S, Grenèche JM, Ulhaq-Bouillet C, Legaré P, et al. Hydrothermal Synthesis of Monodisperse Magnetite Nanoparticles. Chem Mater. 2006;18(18):4399-4404.
24. Park SY, Ahn H-W, Chung JW, Kwak S-Y. Magnetic core-hydrophilic shell nanosphere as stability-enhanced draw solute for forward osmosis (FO) application. Desalination. 2016;397:22-29.
25. Al-Hakeim HK, Al-Kazaz FFM, Alobaid HKA. Adsorption of LH, FSH, and TSH on Magnetic Nanoparticles. Journal of Bionanoscience. 2015;9(6):439-447.
26. Ansari SAMK, Ficiarà E, Ruffinatti FA, Stura I, Argenziano M, Abollino O, et al. Magnetic Iron Oxide Nanoparticles: Synthesis, Characterization and Functionalization for Biomedical Applications in the Central Nervous System. Materials (Basel, Switzerland). 2019;12(3):465.
27. Berghel H. Using the WWW Test Pattern to check HTML client compliance. Computer. 1995;28(9):63-65.
28. Abd El-wahaab B, Elgendy K, El-didamony A. Synthesis and characterization of new azo-dye reagent and using to spectrophotometric determination of samarium(III) in some industrial and blood samples. Chemical Papers. 2019;74(5):1439-1448.
29. Gries W, Leng G. Analytical determination of specific 4,4'-methylene diphenyl diisocyanate hemoglobin adducts in human blood. Analytical and Bioanalytical Chemistry. 2013;405(23):7205-7213.
30. Asefnejad A, Khorasani MT, Behnamghader A, Farsadzadeh B, Bonakdar S. Manufacturing of biodegradable polyurethane scaffolds based on polycaprolactone using a phase separation method: physical properties and in vitro assay. International journal of nanomedicine. 2011;6:2375-2384.
31. Liu Y, Huang Y, Xiao A, Qiu H, Liu L. Preparation of Magnetic Fe_3O_4/MIL-88A Nanocomposite and Its Adsorption Properties for Bromophenol Blue Dye in Aqueous Solution. Nanomaterials (Basel, Switzerland). 2019;9(1):51.
32. Maryamdokht Taimoory S, F. Trant J, Rahdar A, Aliahmad M, Sadeghfar F, Hashemzaei M. Importance of the Inter-Electrode Distance for the Electrochemical Synthesis of Magnetite Nanoparticles: Synthesis, Characterization,

Computational Modelling, and Cytotoxicity. e-Journal of Surface Science and Nanotechnology. 2017;15(0):31-39.
33. Demir A, Topkaya R, Baykal A. Green synthesis of superparamagnetic Fe_3O_4 nanoparticles with maltose: Its magnetic investigation. Polyhedron. 2013;65:282-287.
34. Azizi A. Green Synthesis of Fe_3O_4 Nanoparticles and Its Application in Preparation of Fe_3O_4/Cellulose Magnetic Nanocomposite: A Suitable Proposal for Drug Delivery Systems. Journal of Inorganic and Organometallic Polymers and Materials. 2020;30(9):3552-3561.
35. Miztani E. Stochastic Interpretation for Whack-A-Mole Model. Global Journal of Pure and Applied Mathematics. 2017;13(11):7829.
36. Kurnaz Yetim N, Kurşun Baysak F, Koç MM, Nartop D. Characterization of magnetic Fe_3O_4@SiO_2 nanoparticles with fluorescent properties for potential multipurpose imaging and theranostic applications. Journal of Materials Science: Materials in Electronics. 2020;31(20):18278-18288.
37. Jafari Eskandari M, Hasanzadeh I. Size-controlled synthesis of Fe_3O_4 magnetic nanoparticles via an alternating magnetic field and ultrasonic-assisted chemical co-precipitation. Materials Science and Engineering: B. 2021;266:115050.
38. Na Y, Yang S, Lee S. Evaluation of citrate-coated magnetic nanoparticles as draw solute for forward osmosis. Desalination. 2014;347:34-42.
39. Wu W, He Q, Jiang C. Magnetic iron oxide nanoparticles: synthesis and surface functionalization strategies. Nanoscale research letters. 2008;3(11):397-415.
40. Boudouh D, Ikram R, Mohamed Jan B, Simon Cornelis Metselaar H, Hamana D, Kenanakis G. Synthesis, Characterization and Filtration Properties of Ecofriendly Fe_3O_4 Nanoparticles Derived from Olive Leaves Extract. Materials (Basel, Switzerland). 2021;14(15):4306.
41. Mehdipour M, Ebrahimian Pirbazari A, Khayati G. Cobalt photodeposition on Fe_3O_4/TiO_2 as a novel magnetically separable visible-light-driven photocatalyst for efficient degradation of 2,4-dichlorophenol. DESALINATION AND WATER TREATMENT. 2019;155:329-340.
42. Darwish MSA, Al-Harbi LM. Self-heating properties of iron oxide nanoparticles prepared at room temperature via ultrasonic-assisted co-precipitation process. Soft Materials. 2021;20(1):35-44.
43. Varenne F, Coty JB, Botton J, Legrand FX, Hillaireau H, Barratt G, et al. Evaluation of zeta potential of nanomaterials by electrophoretic light scattering: Fast field reversal versus Slow field reversal modes. Talanta. 2019;205:120062.
44. Sun J-Z, Sun Y-C, Sun L. Synthesis of surface modified Fe_3O_4 super paramagnetic nanoparticles for ultra sound examination and magnetic resonance imaging for cancer treatment. J Photochem Photobiol B: Biol. 2019;197:111547.
45. Ahmadi S, Fazilati M, Nazem H, Mousavi SM. Green Synthesis of Magnetic Nanoparticles Using Satureja hortensis Essential Oil toward Superior Antibacterial/Fungal and Anticancer Performance. BioMed research international. 2021;2021:8822645-8822645.
46. Dhavale RP, Dhavale RP, Sahoo SC, Kollu P, Jadhav SU, Patil PS, et al. Chitosan coated magnetic nanoparticles as carriers of anticancer drug Telmisartan: pH-responsive controlled drug release and cytotoxicity studies. Journal of Physics and Chemistry of Solids. 2021;148:109749.
47. Ajala MA. Development of Titanium Dioxide Pillared Clay Adsorbent for Removal of Lead (II), Zinc (II), and Copper (II) ions from Aqueous Solution. UNIOSUN Journal of Engineering and Environmental Sciences. 2022;4(1).
48. Kalaivani SS, Muthukrishnaraj A, Sivanesan S, Ravikumar L. Novel hyperbranched polyurethane resins for the removal of heavy metal ions from aqueous solution. Process Saf Environ Prot. 2016;104:11-23.
49. Ibrahim MNM, Ngah WSW, Norliyana MS, Daud WRW, Rafatullah M, Sulaiman O, et al. A novel agricultural waste adsorbent for the removal of lead (II) ions from aqueous solutions. J Hazard Mater. 2010;182(1-3):377-385.
50. Singh S, Ma L, Hendry M. Characterization of aqueous lead removal by phosphatic clay: Equilibrium and kinetic studies. J Hazard Mater. 2006;136(3):654-662.
51. Mataka LM, Henry EMT, Masamba WRL, Sajidu SM. Lead remediation of contaminated water using Moringa Stenopetala and Moringa oleifera seed powder. International Journal of Environmental Science & Technology. 2006;3(2):131-139.